Electronic transport properties of graphene nanoribbons

Electronic transport properties of graphene nanoribbons

New Journal of Physics
The open-access journal for physics

Electronic transport properties of graphene nanoribbons

Katsunori Wakabayashi[1,2,5], **Yositake Takane**[3], **Masayuki Yamamoto**[1] **and Manfred Sigrist**[4]

[1] International Center for Materials Nanoarchitectonics (MANA), National Institute for Materials Science (NIMS), Namiki 1-1, Tsukuba 305-0044, Japan
[2] PRESTO, Japan Science and Technology Agency (JST), Kawaguchi 332-0012, Japan
[3] Department of Quantum Matter, AdSM, Hiroshima University, Higashi-Hiroshima 739-8530, Japan
[4] Theoretische Physik, ETH-Zürich, Zürich CH-8093, Switzerland
E-mail: ka.wakaba@gmail.com

New Journal of Physics **11** (2009) 095016 (21pp)
Received 25 May 2009
Published 30 September 2009
Online at http://www.njp.org/
doi:10.1088/1367-2630/11/9/095016

Abstract. We will present a brief overview of the electronic and transport properties of graphene nanoribbons focusing on the effect of edge shapes and impurity scattering. The low-energy electronic states of graphene have two non-equivalent massless Dirac spectra. The relative distance between these two Dirac points in the momentum space and edge states due to the existence of zigzag-type graphene edges is a deciding factor in the electronic and transport properties of graphene nanoribbons. In graphene nanoribbons with zigzag edges (zigzag nanoribbons), two valleys related to each Dirac spectrum are well separated in momentum space. The propagating modes in each valley contain a single chiral mode originating from a partially flat band at the band center. This feature gives rise to a perfectly conducting channel in the disordered system, if impurity scattering does not connect the two valleys, i.e. for long-range impurity (LRI) potentials. Ribbons with short-range impurity potentials, however, display ordinary localization behavior through inter-valley scattering. On the other hand, the low-energy spectrum of graphene nanoribbons with armchair edges (armchair nanoribbons) is described as the superposition of two non-equivalent Dirac points of graphene. In spite of the lack of two well separated valley structures, the single-channel transport subjected to LRIs is nearly perfectly

[5] Author to whom any correspondence should be addressed.

conducting, where the backward scattering matrix elements in the lowest order vanish as a manifestation of internal phase structures of the wave function. For the multi-channel energy regime, however, conventional exponential decay of the averaged conductance occurs. Symmetry considerations lead to the classification of disordered zigzag ribbons into the unitary class for LRIs, and the orthogonal class for short-range impurities. Since inter-valley scattering is not completely absent, armchair nanoribbons can be classified into the orthogonal universality class irrespective of the range of impurities.

Contents

1. Introduction

Recently, graphene, a single-layer hexagonal lattice of carbon atoms, has emerged as a fascinating system for fundamental studies in condensed matter physics, as well as a promising candidate material for future applications in nanoelectronics and molecular devices [1]. The honeycomb crystal structure of single-layer graphene consists of two non-equivalent sublattices and results in a unique band structure for the itinerant π-electrons near the Fermi energy that behave as massless Dirac fermions. The valence and conduction bands touch conically at two non-equivalent Dirac points, called $\boldsymbol{K}_+$ and $\boldsymbol{K}_-$ points, which form a time-reversed pair, i.e. opposite chirality. The chirality and a Berry phase of π at the two Dirac points provide an environment for highly unconventional and fascinating two-dimensional electronic properties [2], such as the half-integer quantum Hall effect [3], the absence of backward scattering [4, 5], and π-phase shift of the Shubnikov–de Haas oscillations [6].

The successive miniaturization of graphene electronic devices inevitably demands clarification of the edge effects on the electronic structures and electronic transport properties of nanometer-sized graphene. The presence of edges in graphene has strong implications for the low-energy spectrum of the π-electrons [7]–[9]. There are two basic shapes of edges, *armchair* and *zigzag*, that determine the properties of graphene ribbons. It was shown that

ribbons with zigzag edges (zigzag ribbons) possess localized edge states with energies close to the Fermi level [7]–[10]. These edge states correspond to non-bonding wave functions, where the amplitudes of the edge states reside on one sublattice only [7]. In contrast, edge states are completely absent for ribbons with armchair edges. Recent experiments support the evidence for edge-localized states [11, 12]. Also, graphene nanoribbons can experimentally be produced by using lithography techniques and chemical techniques [13]–[17].

The electronic transport through graphene nanoribbons shows a number of intriguing phenomena such as zero-conductance Fano resonances [18, 19], valley filtering [20], half-metallic conduction [21], the spin Hall effect [22] and a perfectly conducting channel (PCC) [23]. Recent studies also clarify the unconventional transport through graphene junctions, quantum point contact and heterojunctions [19], [24]–[44]. It is also expected that the edge states play an important role in the magnetic properties in nanometer-sized graphite systems, because of their relatively large contribution to the density of states at the Fermi energy [7, 9], [45]–[56]. Recent studies explore the robustness of edge states to size and geometries [56]–[58], [60], and various edge structures and modifications [56, 59].

Since graphene nanoribbons and carbon nanotubes can be viewed as a new class of quantum wires, one might expect that random impurities inevitably cause Anderson localization, i.e. conductance decays exponentially with increasing system length L and eventually vanishes in the limit of $L \to \infty$. However, it was shown that zigzag nanoribbons and armchair nanotubes subjected to long-range impurities (LRIs) possess a PCC [23, 61]. Recent studies show that PCCs can be stabilized in two standard universality classes. One is the symplectic universality class with an odd number of conducting channels [61]–[63], and the other is the unitary universality class with an imbalance between the numbers of conducting channels in two propagating directions [23, 64, 65]. The symplectic class consists of systems having time-reversal symmetry (TRS) without spin-rotation invariance, while the unitary class is characterized by the absence of time-reversal symmetry [66].

In this paper, we will give a brief overview of the electronic transport properties of disordered graphene nanoribbons. In zigzag nanoribbons, the edge states play an important role, since they appear as special modes with partially flat bands and, under certain conditions, lead to chiral modes separately in the two valleys. There is one such mode of opposite orientation in each of the two valleys of propagating modes, which are well separated in k-space. The key result of this study is that for disorder without inter-valley scattering a single PCC emerges introduced by the presence of these chiral modes. This effect disappears as soon as inter-valley scattering is possible. On the other hand, the low-energy spectrum of graphene nanoribbons with armchair edges (armchair nanoribbons) is described as the superposition of two non-equivalent Dirac points of graphene. In spite of the lack of two well separated valley structures, the single-channel transport subjected to LRIs is nearly perfectly conducting, where the backward scattering matrix elements in the lowest order vanish as a manifestation of internal phase structures of the wave function [67]. For the multi-channel energy regime, however, conventional exponential decay of the averaged conductance occurs. Symmetry considerations lead to the classification of disordered zigzag ribbons into the unitary class for LRIs, and the orthogonal class for short-range impurities (SRIs). Since inter-valley scattering is not completely absent, armchair nanoribbons can be classified into the orthogonal universality class irrespective of the range of impurities.

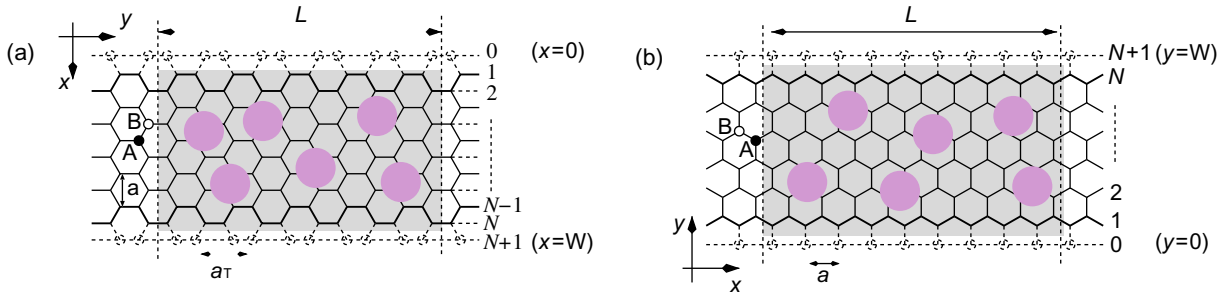

Figure 1. Structure of graphene nanoribbon with (a) armchair edges (armchair ribbon) and (b) zigzag edges (zigzag ribbon). The lattice constant is a and N defines the ribbon width. The circles with dashed lines indicate the missing carbon atoms for the edge boundary condition of the massless Dirac equation. The disordered region with randomly distributed impurities lies in the shaded region and has the length L (see text in section 3). Randomly distributed circles schematically represent the LRIs.

2. Electronic states of graphene and nanoribbons

2.1. Tight-binding model and edge states

There are two typical shapes of a graphene edge, called *armchair* and *zigzag*. The two edges have 30° difference in their cutting direction. Here we briefly discuss the way that the graphene edges drastically change the π-electronic structures [7]. In particular, a zigzag edge provides the localized edge state, while an armchair edge does not show such localized states.

A simple and useful model to study the edge and size effect is one of the graphene ribbon models as shown in figures 1(a) and (b). We define the width of graphene ribbons as N, where N stands for the number of the dimer (two carbon sites) lines for the armchair ribbon and by the number of the zigzag lines for the zigzag ribbon, respectively. It is assumed that all dangling bonds at graphene edges are terminated by hydrogen atoms, and thus make no contribution to the electronic states near the Fermi level. We employ a single-orbital tight-binding model for the π-electron network. The Hamiltonian is written as,

$$H = -t \sum_{\langle i,j \rangle} c_i^\dagger c_j + \sum_i V_i c_i^\dagger c_i, \tag{1}$$

where the operator $c_i^\dagger$ creates a π-electron on the site i. $\langle i,j \rangle$ denotes the summation over the nearest-neighbor sites. t, the transfer integrals between all the nearest-neighbor sites, are set to be unity for simplicity. This is sufficient to show the intrinsic difference in the electronic states originating from the topological nature of each system. The value of t is considered to be about 2.75 eV in a graphene system. The second term in equation (1) represents the impurity potential; $V_\mathrm{i} = V(\boldsymbol{r}_\mathrm{i})$ is the impurity potential at a position $\boldsymbol{r}_\mathrm{i}$. The effect of impurity potential on the electronic transport properties will be discussed in the next section.

Prior to the discussion of the π-electronic states of graphene nanoribbons, we shall briefly review the π-band structure of a graphene sheet [68]. To diagonalize the Hamiltonian for a graphene sheet, we use a basis of the two-component spinor, $c_\mathbf{k}^\dagger = (c_{\mathrm{A}\mathbf{k}}^\dagger, c_{\mathrm{B}\mathbf{k}}^\dagger)$, which is the Fourier transform of $(c_{i\in\mathrm{A}}^\dagger, c_{i\in\mathrm{B}}^\dagger)$. Let $\boldsymbol{\tau_1}$, $\boldsymbol{\tau_2}$ and $\boldsymbol{\tau_3}$ be the displacement vectors from a B site to its three

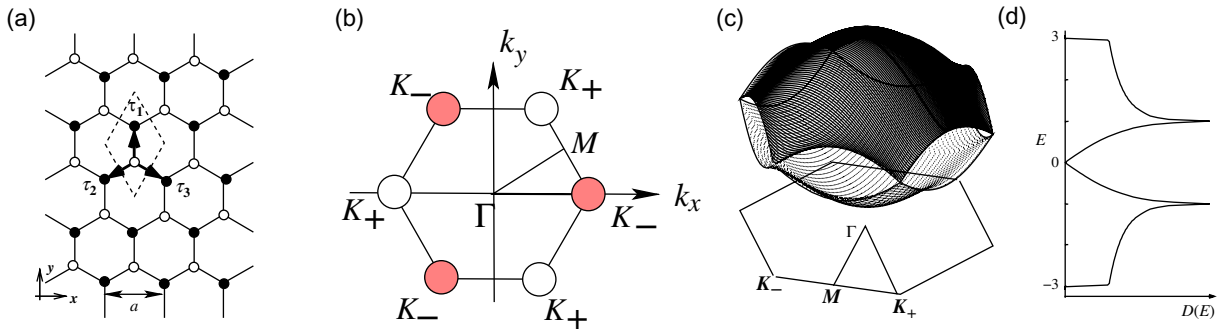

Figure 2. (a) A graphene sheet in real space, where the black (white) circles mean the A(B)-sublattice site. a is the lattice constant. Here $\boldsymbol{\tau_1} = (0, a/\sqrt{3})$, $\boldsymbol{\tau_2} = (-a/2, -a/2\sqrt{3})$, and $\boldsymbol{\tau_3} = (a/2, -a/2\sqrt{3})$. (b) First BZ of graphene. $\boldsymbol{K}_+ = \frac{2\pi}{a}(\frac{1}{3}, \frac{1}{\sqrt{3}})$, $\boldsymbol{K}_- = \frac{2\pi}{a}(\frac{2}{3}, 0)$, $\boldsymbol{\Gamma} = (0, 0)$. (c) The π band structure and (d) the density of states of the graphene sheet. The valence and conduction bands make contact at the degeneracy point $\boldsymbol{K}_\pm$.

nearest-neighbor A sites, defined so that $\hat{z} \cdot \boldsymbol{\tau_1} \times \boldsymbol{\tau_2}$ is positive (figure 2(a)). $\hat{z}$ is the normal vector to the graphene sheet. In this representation, the Hamiltonian is written as $H = \sum_{\mathbf{k}} \mathbf{c}_{\mathbf{k}}^\dagger H_{\mathbf{k}} \mathbf{c}_{\mathbf{k}}$ and

$$H_{\mathbf{k}} = -t \sum_{i=1}^{3} \left(\cos(\boldsymbol{k} \cdot \boldsymbol{\tau}_i) \hat{\sigma}_x + \sin(\boldsymbol{k} \cdot \boldsymbol{\tau}_i) \hat{\sigma}_y \right), \tag{2}$$

where $\hat{\boldsymbol{\sigma}} = (\hat{\sigma}_x, \hat{\sigma}_y, \hat{\sigma}_z)$ are the Pauli matrices. Then, the energy eigenvalues are $E_{\mathbf{k}}^{\pm} = \pm t |\sum_{i=1}^{3} \exp(\boldsymbol{k} \cdot \boldsymbol{\tau}_i)|$. Since one carbon site has one π-electron on average, only the $E_{\mathbf{k}}^{-}$-band is completely occupied.

In figures 2(b)–(d), the first Brillouin zone (BZ) of the graphene lattice, the energy dispersion of π-bands in the first BZ and the corresponding density of states are depicted, respectively. Near the Γ point, both valence and conduction bands have the quadratic form of k_x and k_y, i.e. $E_k = \pm(3 - 3|\boldsymbol{k}|^2/4)$. At the M points, the middle points of the sides of the hexagonal BZ, the saddle point of energy dispersion appears and the density of states diverges logarithmically. Near the K point of the corner of the hexagonal first BZ, the energy dispersion is linear in the magnitude of the wave vector, $E_{\mathbf{k}} = \pm\sqrt{3}ta|\boldsymbol{k}|/2$, where the density of states linearly depends on the energy. Here $a(= \sqrt{3}|\boldsymbol{\tau}_i|(i = 1, 2, 3))$ is the lattice constant. The Fermi energy is located at the K points and there is no energy gap at these points, since $E_{\mathbf{k}}$ vanishes at these points by hexagonal symmetry.

The energy band structures of armchair ribbons are shown in figures 3(a)–(c), for three different ribbon widths, together with the density of states. The wavenumber k is normalized by the length of the primitive translation vector of each graphene nanoribbon, and the energy E is scaled by the transfer integral t. The top of the valence band and the bottom of the conduction band are located at $k = 0$. It should be noted that the ribbon width decides whether the system is metallic or semiconducting. As shown in figure 3(b), the system is metallic when $N = 3M - 1$, where M is an integer. For semiconducting ribbons, the direct gap decreases with increasing ribbon width and tends to zero in the limit of very large N. For narrow non-doped metallic armchair nanoribbons, an energy gap can develop due to Peierls instabilities

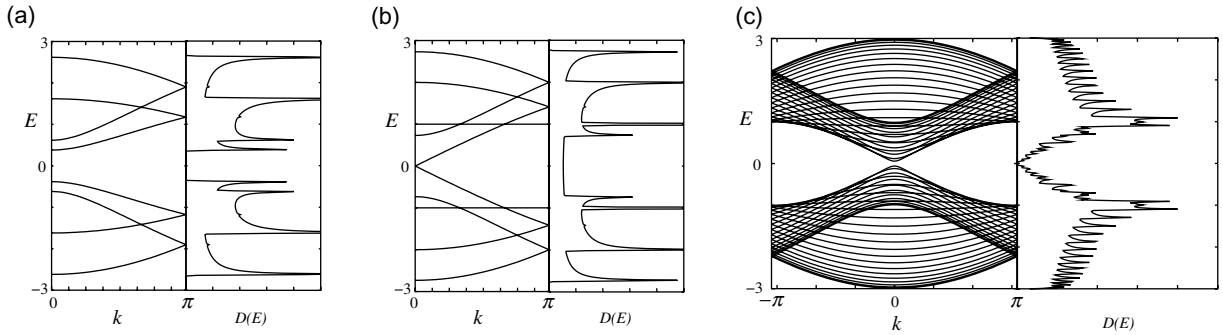

Figure 3. Energy band structure $E(k)$ and density of states $D(E)$ of armchair ribbons of various widths ((a) $N = 4$, (b) 5 and (c) 30).

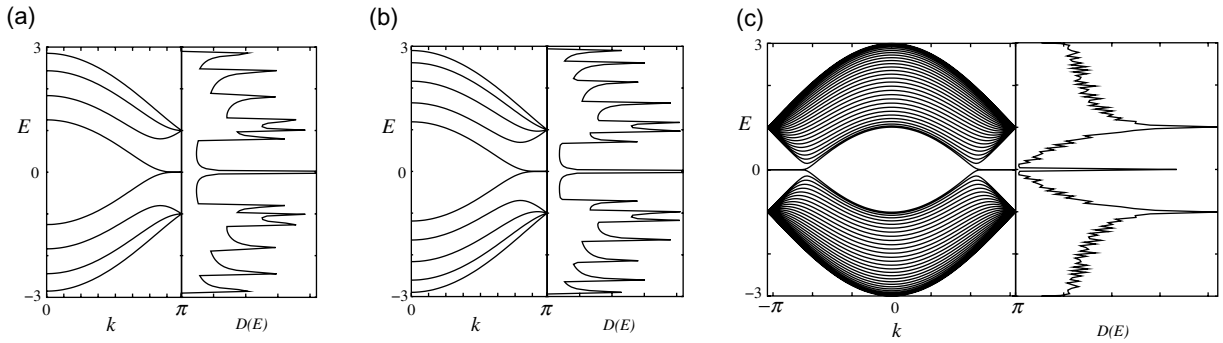

Figure 4. Energy band structure $E(k)$ and density of states $D(E)$ of zigzag ribbons of various widths ((a) $N = 4$, (b) 5 and (c) 30).

toward low temperatures [69], which is consistent with the recent density functional theory calculation [56, 70].

For zigzag ribbons, however, a remarkable feature arises in the band structure, as shown in figures 4(a)–(c). We see that the highest valence band and lowest conduction band are always degenerate at $k = \pi$. It is found that the degeneracy of the center bands at $k = \pi$ does not originate from the intrinsic band structure of the graphene sheet. These two special center bands get flatter with increasing ribbon width. A pair of partial flat bands appears within the region of $2\pi/3 \leqslant |k| \leqslant \pi$, where the bands sit in the vicinity of the Fermi level.

The electronic state in the partial flat bands of the zigzag ribbons can be understood as the localized state near the zigzag edge by examining the charge density distribution [7]–[9], [11, 12]. Here we show that the puzzle for the emergence of the edge state can be solved by considering a semi-infinite graphite sheet with a zigzag edge. First, to show the analytic form, we depict the distribution of charge density in the flat band states for some wavenumbers in figure 5(a)–(d), where the amplitude is proportional to the radius. The wave function has non-bonding character, i.e. finite amplitudes only on one of the two sublattices, which includes the edge sites. It is completely localized at the edge site when $k = \pi$, and starts to gradually penetrate into the inner sites as k deviates from π reaching the extended state at $k = 2\pi/3$.

Considering the translational symmetry, we can start constructing the analytic solution for the edge state by letting the Bloch components of the linear combination of atomic orbitals

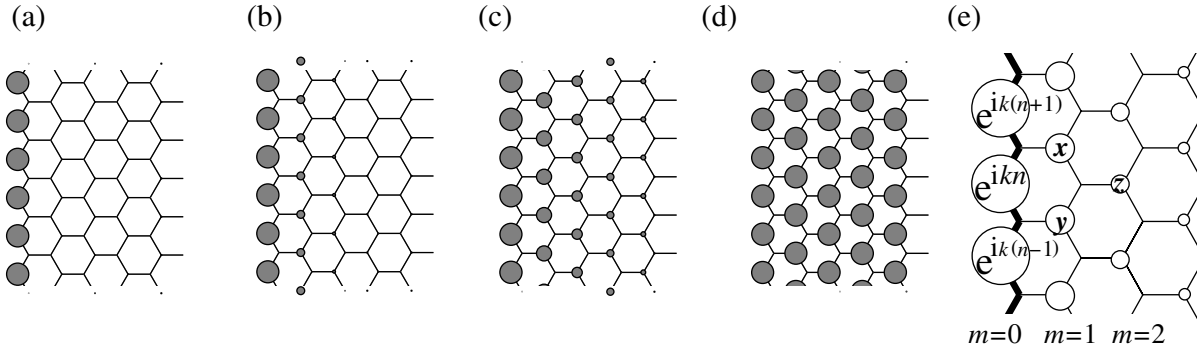

Figure 5. Charge density plot for analytic solution of the edge states in semi-infinite graphite, when (a) $k = \pi$, (b) $8\pi/9$, (c) $7\pi/9$ and (d) $2\pi/3$. (e) An analytic form of the edge state for a semi-infinite graphite sheet with a zigzag edge, emphasized by bold lines. Each carbon site is specified by a location index n on the zigzag chain and by a chain order index m from the edge. The magnitude of the charge density at each site, such as x, y and z, is obtained analytically (see text). The radius of each circle is proportional to the charge density on each site, and a drawing is given for $k = 7\pi/9$.

(LCAO) wave function be $\ldots, e^{ik(n-1)}, e^{ikn}, e^{ik(n+1)}, \ldots$ on successive edge sites, where n denotes a site location on the edge. Then the mathematical condition necessary for the wave function to be exact for $E = 0$ is that the total sum of the components of the complex wave function over the nearest-neighbor sites should vanish. In figure 5(e), the above condition is $e^{ik(n+1)} + e^{ikn} + x = 0$, $e^{ikn} + e^{ik(n-1)} + y = 0$ and $x + y + z = 0$. Therefore, the wave function components x, y and z are found to be $D_k e^{ik(n+1/2)}$, $D_k e^{ik(n-1/2)}$ and $D_k^2 e^{ikn}$, respectively. Here $D_k = -2\cos(k/2)$. We can thus see that the charge density is proportional to $D_k^{2(m-1)}$ at each non-nodal site of the mth zigzag chain from the edge. Then the convergence condition of $|D_k| \leqslant 1$ is required, for otherwise the wave function would diverge in a semi-infinite graphite sheet. This convergence condition defines the region $2\pi/3 \leqslant |k| \leqslant \pi$ where the flat band appears.

2.2. Massless Dirac equation

We briefly discuss here the relation between the massless Dirac spectrum of graphene and low-energy electronic states of nanoribbons. The electronic states near the two non-equivalent Dirac points ($\boldsymbol{K}_{\pm}$) can be described by 4×4 Dirac equation, i.e.

$$H_{\boldsymbol{k}\cdot\boldsymbol{p}}\boldsymbol{F}(\boldsymbol{r}) = \epsilon \boldsymbol{F}(\boldsymbol{r}) \tag{3}$$

with

$$H_{\boldsymbol{k}\cdot\boldsymbol{p}} = \begin{pmatrix} 0 & \gamma(\hat{k}_x - \mathrm{i}\hat{k}_y) & 0 & 0 \\ \gamma(\hat{k}_x + \mathrm{i}\hat{k}_y) & 0 & 0 & 0 \\ 0 & 0 & 0 & \gamma(\hat{k}_x + \mathrm{i}\hat{k}_y) \\ 0 & 0 & \gamma(\hat{k}_x - \mathrm{i}\hat{k}_y) & 0 \end{pmatrix} \tag{4}$$

and

$$\boldsymbol{F}(\boldsymbol{r}) = \begin{pmatrix} F_{\mathrm{A}}^{\boldsymbol{K}_+}(\boldsymbol{r}) \\ F_{\mathrm{B}}^{\boldsymbol{K}_+}(\boldsymbol{r}) \\ F_{\mathrm{A}}^{\boldsymbol{K}_-}(\boldsymbol{r}) \\ F_{\mathrm{B}}^{\boldsymbol{K}_-}(\boldsymbol{r}) \end{pmatrix}. \tag{5}$$

Here, $\hat{k}_x(\hat{k}_y)$ is a wavevector operator, and can be replaced by $\hat{\boldsymbol{k}} \to -\mathrm{i}\hat{\nabla}$ in the absence of magnetic field. γ is a band parameter, which satisfies $\gamma = \sqrt{3}ta/2$. $F_{\mathrm{A}}^{\boldsymbol{K}_\pm}(\boldsymbol{r})$ and $F_{\mathrm{B}}^{\boldsymbol{K}_\pm}(\boldsymbol{r})$ are the envelope functions near $\boldsymbol{K}_\pm$ points for A and B sublattices, which slowly vary in the length scale of the lattice constant. We can rewrite the above effective mass Hamiltonian by using the Pauli matrices $\tau^{x,y,z}$ for valley space ($\boldsymbol{K}_\pm$) as

$$H_{\boldsymbol{k}\cdot\boldsymbol{p}} = \gamma\left[\hat{k}_x(\sigma^x \otimes \tau^0) + \hat{k}_y(\sigma^y \otimes \tau^z)\right]. \tag{6}$$

Here, τ^0 is the 2×2 identity matrix. We can easily obtain the linear energy spectrum for graphene as

$$\epsilon = s\gamma|k| \quad \text{with} \quad s = \pm 1, \tag{7}$$

and the corresponding wave functions with the definition of $\Phi_{\boldsymbol{K}_\pm} = [F_{\boldsymbol{K}_\pm \mathrm{A}}, F_{\boldsymbol{K}_\pm \mathrm{B}}]$ are

$$\Phi_{\boldsymbol{K}_\pm} = \frac{1}{\sqrt{2}}\begin{pmatrix} s \\ \mathrm{e}^{\pm \mathrm{i}\phi_k} \end{pmatrix} \mathrm{e}^{\mathrm{i}\boldsymbol{k}\cdot\boldsymbol{r}}. \tag{8}$$

Here

$$\mathrm{e}^{\pm \mathrm{i}\phi_k} = \frac{k_x \pm \mathrm{i}k_y}{|k_x + \mathrm{i}k_y|}. \tag{9}$$

2.2.1. Zigzag nanoribbons. The low-energy electronic states for zigzag nanoribbons can also be described starting from the Dirac equation [10, 71]. Since the outermost sites along the first (Nth) zigzag chain are B(A)-sublattice, an imbalance between two sublattices occurs at the zigzag edges leading to the boundary conditions

$$\phi_{\boldsymbol{K}_\pm \mathrm{A}}(\boldsymbol{r}_{[0]}) = 0, \quad \phi_{\boldsymbol{K}_\pm \mathrm{B}}(\boldsymbol{r}_{[N+1]}) = 0, \tag{10}$$

where $\boldsymbol{r}_{[i]}$ stands for the coordinate at the ith zigzag chain. The energy eigenvalue and wavenumber is given by the following relation:

$$\varepsilon = \pm(\eta - k)\mathrm{e}^{\eta W}, \tag{11}$$

where $\eta = \sqrt{k^2 - \varepsilon}$. It can be shown that the valley near $k = 3\pi/2a$ in figure 1(b) originates from the $\boldsymbol{K}_+$-point, the other valley at $k = -3\pi/2a$ from the $\boldsymbol{K}_-$-point [10, 71].

2.2.2. Armchair nanoribbons. The boundary condition of armchair nanoribbons projects $\boldsymbol{K}_+$ and $\boldsymbol{K}_-$ states into the Γ point in the first BZ as can be seen in figure 2(b). Thus, the low-energy states for armchair nanoribbons are the superposition of $\boldsymbol{K}_+$ and $\boldsymbol{K}_-$ states. The boundary condition for armchair nanoribbons [71] can be written as

$$[F_{\mathrm{A}}^{+}(x, y) + F_{\mathrm{A}}^{-}(x, y)]|_{x=0,W} = 0, \tag{12}$$

$$[F_{\mathrm{B}}^{+}(x, y) - F_{\mathrm{B}}^{-}(x, y)]|_{x=0,W} = 0. \tag{13}$$

If the ribbon width W satisfies the condition of $W = (3/2)(N_w + 1)a$ with $N_w = 0, 1, 2, \ldots$, the system becomes metallic with the linear spectrum. The corresponding energy is given by

$$\epsilon_{n,k,s} = s\gamma\sqrt{\kappa_n^2 + k^2}, \tag{14}$$

where $\kappa_n = \frac{2\pi n}{3(N_w+1)a}$, $n = 0, \pm 1, \pm 2, \ldots$ and $s = \pm$. The $n = 0$ mode is the lowest linear subband for metallic armchair ribbons. The energy gap (Δ_s) to the first parabolic subband of $n = 1$ is given as

$$\Delta_s = 4\pi\gamma/3(N_w + 1)a, \tag{15}$$

which is inversely proportional to ribbon width. It should be noted that a small energy gap can be acquired due to the Peierls distortion for half-filling at low temperatures [69, 70], but such an effect is not relevant for single-channel transport in the doped energy regime.

2.3. Edge boundary condition and inter-valley scattering

Now we discuss the relation between the inter-valley scattering and edge boundary condition. According to [5], the impurity potential can be included in the massless Dirac equation by adding the following potential term $\hat{U}_{\rm imp}$ described as

$$\hat{U}_{\rm imp} = \begin{pmatrix} u_{\rm A}(\boldsymbol{r}) & 0 & u'_{\rm A}(\boldsymbol{r}) & 0 \\ 0 & u_{\rm B}(\boldsymbol{r}) & 0 & -u'_{\rm B}(\boldsymbol{r}) \\ u'_{\rm A}(\boldsymbol{r})^* & 0 & u_{\rm A}(\boldsymbol{r}) & 0 \\ 0 & -u'_{B}(\boldsymbol{r})^* & 0 & u_{\rm B}(\boldsymbol{r}) \end{pmatrix}, \tag{16}$$

with

$$u_X(\boldsymbol{r}) = \sum_{\boldsymbol{R}_X} g\,(\boldsymbol{r} - \boldsymbol{R}_X)\,\tilde{u}_X\,(\boldsymbol{R}_X), \tag{17}$$

$$u'_X(\boldsymbol{r}) = \sum_{\boldsymbol{R}_X} g\,(\boldsymbol{r} - \boldsymbol{R}_X)\,\mathrm{e}^{-\mathrm{i}2\boldsymbol{K}\cdot\boldsymbol{R}_X}\tilde{u}_X\,(\boldsymbol{R}_X), \tag{18}$$

where $\tilde{u}_X(\boldsymbol{R}_X)$ is the local potential due to impurities for $X = A$ or B. Here $g(\boldsymbol{R})$ with the normalization condition of $\sum_{\boldsymbol{R}} g(\boldsymbol{R}) = 1$ is a real function, which has an appreciable amplitude in the region where $|\boldsymbol{R}|$ is smaller than a few times of the lattice constant, and decays rapidly with increasing $|\boldsymbol{R}|$. For convenience we distinguish the impurity into two types by the range of the impurity potential: one is LRI if the range of impurity potential is much larger than the lattice constant and the other is SRI if the range of impurity is smaller than the lattice constant.

If only the LRIs are present, we can approximate $u_{\rm A}(\boldsymbol{r}) = u_{\rm B}(\boldsymbol{r}) \equiv u(\boldsymbol{r})$ and $u'_{\rm A}(\boldsymbol{r}) = u'_{\rm B}(\boldsymbol{r}) \equiv u'(\boldsymbol{r})$. In the case of carbon nanotubes and zigzag nanoribbons, $u'_X(\boldsymbol{r})$, $u'_X(\boldsymbol{r})$ vanishes after the summation over $\boldsymbol{R}_X$ in equation (18) since the phase factor $\mathrm{e}^{-\mathrm{i}2\boldsymbol{K}\cdot\boldsymbol{R}_X}$ strongly oscillates in the x-direction. This means that the two valleys are independent and one can only focus on either the $\boldsymbol{K}_+$ or $\boldsymbol{K}_-$ valley. *Thus LRIs do not induce inter-valley scattering for zigzag nanoribbons.*

However, this cancelation is not complete in an armchair nanoribbon because the averaging over the x-direction is restricted to the finite width of W. This means that we cannot neglect the contribution from scatterers particularly in the vicinity of the edges to $u'_X(\boldsymbol{r})$. *This means that inter-valley scattering does not vanish even in the case of LRI in the armchair nanoribbons.*

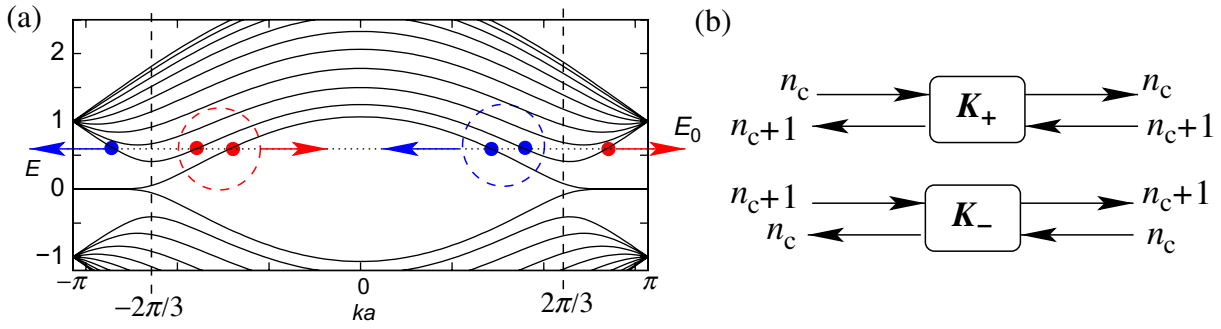

Figure 6. (a) Energy dispersion of zigzag ribbon with $N = 10$. The valleys in the energy dispersion near $k = 2\pi/3a$ ($k = -2\pi/3a$) originate from the Dirac $\boldsymbol{K}_+(\boldsymbol{K}_-)$-point of graphene. The red-filled (blue-unfilled) circles denote the right (left)-moving open channel at the energy E_0 (dashed horizontal line). In the left (right) valley, the degeneracy between right and left moving channels is missing due to one excess right (left)-going mode. The TRS under the intra-valley scattering is also broken. (b) Schematic figure of scattering geometry at $\boldsymbol{K}_+$ and $\boldsymbol{K}_-$ points in zigzag nanoribbons, where a single excess right-going mode exists for the $\boldsymbol{K}_-$ point, but a single excess left-going mode exists for the $\boldsymbol{K}_-$ point. Here $n_c = 0, 1, 2, \ldots$.

3. Electronic transport properties

We numerically discuss the electronic transport properties of the disordered graphene nanoribbons. In general, electron scattering in a quantum wire is described by the scattering matrix [66]. Through the scattering matrix $\boldsymbol{S}$, the amplitudes of the scattered waves $\boldsymbol{O}$ are related to the incident waves $\boldsymbol{I}$,

$$\begin{pmatrix} \boldsymbol{O}_L \\ \boldsymbol{O}_R \end{pmatrix} = \boldsymbol{S} \begin{pmatrix} \boldsymbol{I}_L \\ \boldsymbol{I}_R \end{pmatrix} = \begin{pmatrix} \boldsymbol{r} & \boldsymbol{t}' \\ \boldsymbol{t} & \boldsymbol{r}' \end{pmatrix} \begin{pmatrix} \boldsymbol{I}_L \\ \boldsymbol{I}_R \end{pmatrix}. \tag{19}$$

Here, $\boldsymbol{r}$ and $\boldsymbol{r}'$ are reflection matrices, $\boldsymbol{t}$ and $\boldsymbol{t}'$ are transmission matrices, L and R denote the left and right lead lines. The Landauer–Büttiker formula [73] relates the scattering matrix to the conductance of the sample. The electrical conductance is calculated using the Landauer–Büttiker formula,

$$G(E) = \frac{e^2}{\pi\hbar}\mathrm{Tr}(\boldsymbol{t}\boldsymbol{t}^\dagger) = \frac{e^2}{\pi\hbar}g(E). \tag{20}$$

Here the transmission matrix $\boldsymbol{t}(E)$ is calculated by means of the recursive Green function method [18, 74]. For simplicity, throughout this paper, we evaluate electronic conductance in units of quantum conductance ($e^2/\pi\hbar$), i.e. dimensionless conductance $g(E)$. We would like to mention that recently the edge disorder effect on the electronic transport properties of graphene nanoribbons was studied using a similar approach [75]–[77].

3.1. One-way excess channel system

In this subsection, we consider the conductance of zigzag nanoribbons in the clean limit, which is simply given by the number of the conducting channel. As can be seen in figure 6(a), there

is always one excess left-going channel in the right valley ($\boldsymbol{K}_+$) within the energy window of $|E| \leqslant 1$. Analogously, there is one excess right-going channel in the left valley ($\boldsymbol{K}_-$) within the same energy window. Although the number of right-going and left-going channels are balanced as a whole system, if we focus on one of two valleys, there is always one excess channel in one direction, i.e. a chiral mode.

Now let us consider the injection of electrons from left to right through the sample. When the chemical potential is changed from $E = 0$, the quantization rule of the dimensionless conductance ($g_{\boldsymbol{K}_+}$) in the valley of $\boldsymbol{K}_+$ is given as

$$g_{\boldsymbol{K}_+} = n, \tag{21}$$

where $n = 0, 1, 2, \ldots$. The quantization rule in the $\boldsymbol{K}_-$-valley is

$$g_{\boldsymbol{K}_+} = n + 1. \tag{22}$$

Thus, conductance quantization of the zigzag nanoribbon in the clean limit near $E = 0$ has the following odd-number quantization, i.e.

$$g = g_{\boldsymbol{K}_+} + g_{\boldsymbol{K}_-} = 2n + 1. \tag{23}$$

Since we have an excess mode in each valley, the scattering matrix has some peculiar features, which can be seen when we explicitly write the valley dependence in the scattering matrix. By denoting the contribution of the right valley ($\boldsymbol{K}_+$) as +, and that of the left valley ($\boldsymbol{K}_-$) as −, the scattering matrix can be rewritten as

$$\begin{pmatrix} \boldsymbol{O}_L^+ \\ \boldsymbol{O}_L^- \\ \boldsymbol{O}_R^+ \\ \boldsymbol{O}_R^- \end{pmatrix} = \begin{pmatrix} \boldsymbol{r} & \boldsymbol{t}' \\ \boldsymbol{t} & \boldsymbol{r}' \end{pmatrix} \begin{pmatrix} \boldsymbol{I}_L^+ \\ \boldsymbol{I}_L^- \\ \boldsymbol{I}_R^+ \\ \boldsymbol{I}_R^- \end{pmatrix}. \tag{24}$$

Here we should note that the dimension of each column vector is not identical. Let us denote the number of the right-going channel in the valley $\boldsymbol{K}_+$ or the left-going channel in the valley $\boldsymbol{K}_-$ as n_c. For example, $n_c = 1$ at $E = E_0$ in figure 6(a). Figure 6(b) shows the schematic figure of scattering geometry for $\boldsymbol{K}_+$ and $\boldsymbol{K}_-$ points. Thus the dimension of the column vectors is given as follows:

$$\begin{cases} \dim(\boldsymbol{I}_L^+) = n_c, & \dim(\boldsymbol{I}_R^+) = n_c + 1, \\ \dim(\boldsymbol{I}_L^-) = n_c + 1, & \dim(\boldsymbol{I}_R^-) = n_c, \end{cases} \tag{25}$$

and

$$\begin{cases} \dim(\boldsymbol{O}_L^+) = n_c + 1, & \dim(\boldsymbol{O}_R^+) = n_c, \\ \dim(\boldsymbol{O}_L^-) = n_c, & \dim(\boldsymbol{O}_R^-) = n_c + 1. \end{cases} \tag{26}$$

Subsequently, the reflection matrices have the following matrix structures:

$$\boldsymbol{r} = \begin{matrix} \\ n_c + 1 \\ n_c \end{matrix} \begin{matrix} \begin{matrix} n_c & n_c + 1 \end{matrix} \\ \begin{pmatrix} \boldsymbol{r}_{++} & \boldsymbol{r}_{+-} \\ \boldsymbol{r}_{-+} & \boldsymbol{r}_{--} \end{pmatrix} \end{matrix}, \tag{27}$$

$$\boldsymbol{r}' = \begin{matrix} \\ n_c \\ n_c + 1 \end{matrix} \begin{matrix} \begin{matrix} n_c + 1 & n_c \end{matrix} \\ \begin{pmatrix} \boldsymbol{r}'_{++} & \boldsymbol{r}'_{+-} \\ \boldsymbol{r}'_{-+} & \boldsymbol{r}'_{--} \end{pmatrix} \end{matrix}. \tag{28}$$

The reflection matrices become non-square when the inter-valley scattering is suppressed, i.e. the off-diagonal submatrices ($\boldsymbol{r}_{+-}$, $\boldsymbol{r}_{-+}$ and so on) are zero.

When the electrons are injected from the left lead of the sample and the inter-valley scattering is suppressed, a system with an excess channel is realized in the $\boldsymbol{K}_-$-valley. Thus, for single valley transport, the $\boldsymbol{r}_{--}$ and $\boldsymbol{r}'_{--}$ are $n_c \times (n_c+1)$ and $(n_c+1) \times n_c$ matrices, respectively, and $\boldsymbol{t}_{--}$ and $\boldsymbol{t}'_{--}$ are $(n_c+1) \times (n_c+1)$ and $n_c \times n_c$ matrices, respectively. Noting the dimensions of $\boldsymbol{r}_{--}$ and $\boldsymbol{r}'_{--}$, we find that $\boldsymbol{r}^\dagger_{--}\boldsymbol{r}_{--}$ and $\boldsymbol{r}'_{--}\boldsymbol{r}'^\dagger_{--}$ have a single zero eigenvalue. Combining this property with the flux conservation relation ($\boldsymbol{S}^\dagger\boldsymbol{S} = \boldsymbol{S}\boldsymbol{S}^\dagger = \boldsymbol{1}$), we arrive at the conclusion that $\boldsymbol{t}_{--}t^\dagger_{--}$ has an eigenvalue equal to unity, which indicates the presence of a PCC only in the right-moving channels. Note that $\boldsymbol{t}'_{--}\boldsymbol{t}'^\dagger_{--}$ does not have such an anomalous eigenvalue. If the set of eigenvalues for $\boldsymbol{t}'_{--}\boldsymbol{t}'^\dagger_{--}$ is expressed as $\{T_1, T_2, \ldots, T_{n_c}\}$, that for $\boldsymbol{t}_{--}\boldsymbol{t}^\dagger_{--}$ is expressed as $\{T_1, T_2, \ldots, T_{n_c}, 1\}$, i.e. a PCC. Thus, the dimensionless conductance g for the right-moving channels is given as

$$g_{\boldsymbol{K}_-} = \sum_{i=1}^{n_c+1} T_i = 1 + \sum_{i=1}^{n_c} T_i, \tag{29}$$

while that for the left-moving channels is

$$g'_{\boldsymbol{K}_-} = \sum_{i=1}^{n_c} T_i. \tag{30}$$

We see that $g_{\boldsymbol{K}_-} = g'_{\boldsymbol{K}_-} + 1$. Since the overall TRS of the system guarantees the following relation:

$$\begin{aligned} g'_{\boldsymbol{K}_+} &= g_{\boldsymbol{K}_-}, \\ g'_{\boldsymbol{K}_-} &= g_{\boldsymbol{K}_+}, \end{aligned} \tag{31}$$

the conductance $g = g_{\boldsymbol{K}_+} + g_{\boldsymbol{K}_-}$ (right-moving) and $g' = g'_{\boldsymbol{K}_+} + g'_{\boldsymbol{K}_-}$ (left-moving) are equivalent. If the probability distribution of $\{T_i\}$ is obtained as a function L, we can describe the statistical properties of g as well as g'. The evolution of the distribution function with increasing L is described by the DMPK (Dorokhov–Mello–Pereyra–Kumar) equation for transmission eigenvalues [65].

In the following, the presence of a PCC in disordered graphene nanoribbons will be demonstrated with the help of numerical calculation. Recently Hirose *et al* pointed out that the Chalker–Coddington model, which possesses non-square reflection matrices with unitary symmetry, gives rise to a PCC [64]. However, systems with an excess channel in one direction were believed difficult to realize. Therefore disordered graphene zigzag nanoribbons with LRI might constitute the first realistic example. It is possible to extend the discussion to a generic multiple-excess channel model, where the m-PCCs ($m = 2, 3, \ldots$) appear [65]. Such systems can be realized by stacking zigzag nanographene ribbons [78]. The electronic transport due to PCC resembles the electronic transport due to a chiral mode in the quantum Hall system. However, it should be noted that PCC due to edge states in zigzag ribbons occurs even without the magnetic field [79, 80].

3.2. Model of impurity potential

As shown in figure 1, the impurities are randomly distributed with a density n_{imp} in the nanoribbons. In our model, we assume that the each impurity potential has a Gaussian form

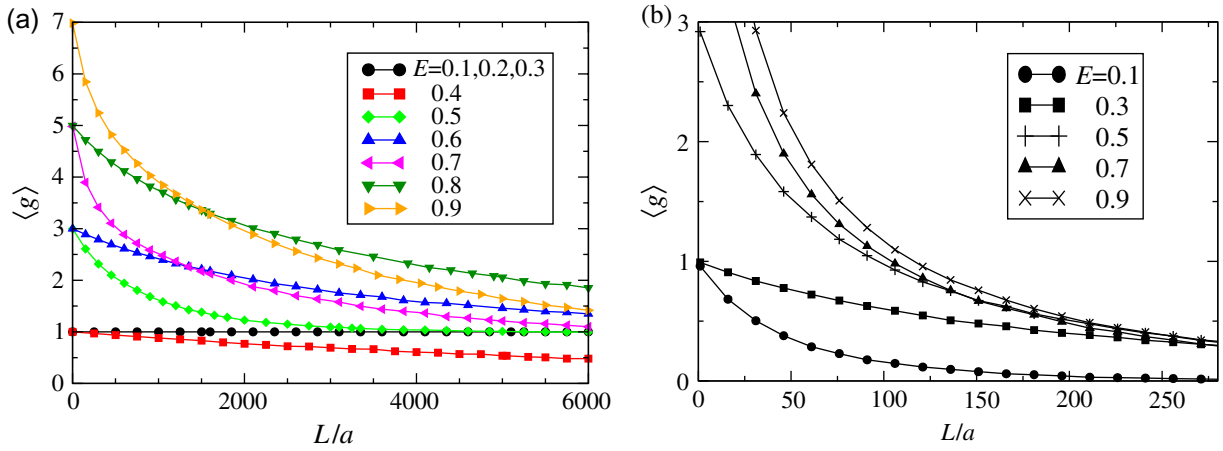

Figure 7. L-dependence of the averaged dimensionless conductance $\langle g\rangle$ for a zigzag nanoribbon with $N = 10$, (a) $d/a = 1.5$ (no inter-valley scattering), (b) $d/a = 0.1$ (inter-valley scattering). Here $u_0 = 1.0$, and $n_{\rm imp} = 0.1$. More than 9000 samples with different impurity configurations are included in the ensemble average.

of a range d

$$V(\boldsymbol{r}_i) = \sum_{\boldsymbol{r_0}\,(\text{random})} u\ \exp\left(-\frac{|\boldsymbol{r}_{\rm i} - \boldsymbol{r}_0|^2}{d^2}\right), \tag{32}$$

where the strength u is uniformly distributed within the range $|u| \leqslant u_M$. Here u_M satisfies the normalization condition:

$$u_M \sum_{\boldsymbol{r}_{\rm i}}^{(\text{full space})} \exp(-\boldsymbol{r}_{\rm i}^2 d^2)/(\sqrt{3}/2) = u_0. \tag{33}$$

In this work, we set $n_{\rm imp} = 0.1$, $u_0 = 1.0$ and $d/a = 1.5$ for LRI and $d/a = 0.1$ for SRI.

3.3. PCC: absence of Anderson localization

We focus first on the case of LRI using a potential with $d/a = 1.5$, which is already sufficient to avoid inter-valley scattering. Figure 7(a) shows the averaged dimensionless conductance as a function of L for different incident energies (Fermi energies), averaging over an ensemble of 40 000 samples with different impurity configurations for ribbons of width $N = 10$. The potential strength and impurity density are chosen to be $u_0 = 1.0$ and $n_{\rm imp} = 0.1$, respectively. As a typical localization effect, we observe that $\langle g\rangle$ gradually decreases with increasing length L (figure 7). However, $\langle g\rangle$ converges to $\langle g\rangle = 1$ for LRIs (figure 7(a)), indicating the presence of a single PCC. It can be seen that $\langle g\rangle(L)$ has an exponential behavior as

$$\langle g\rangle - 1 \sim \exp(-L/\xi) \tag{34}$$

with ξ as the localization length.

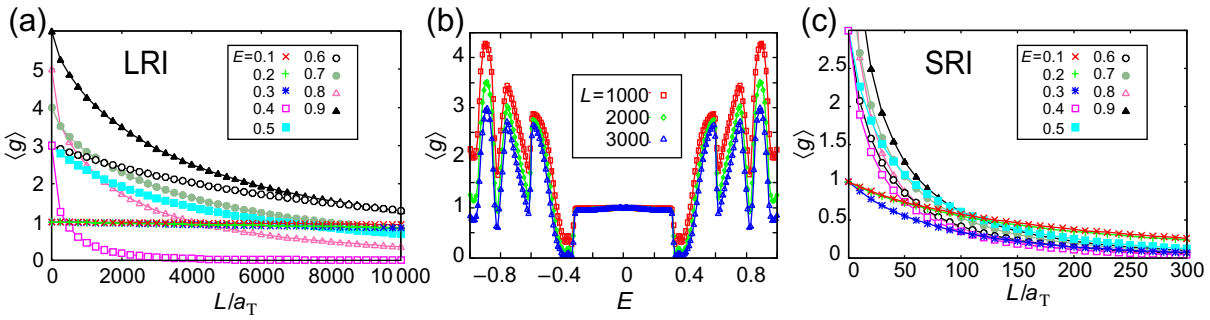

Figure 8. (a) Average conductance $\langle g \rangle$ as a function of the ribbon length L in the presence of LRIs for several different Fermi energies E. Conductance is almost unaffected by impurities for single-channel transport ($E = 0.1, 0.2$ and 0.3), while it shows a conventional exponential decay for multi-channel transport ($E \geqslant 0.4$). Here, $N = 14$, $n_{\mathrm{imp}} = 0.1$ and $d/a = 1.5$. Ensemble average is taken over 10^4 samples. (b) The Fermi energy dependence of $\langle g \rangle$ for LRI. (c) The same as (a) for SRIs. Here, $N = 14$, $n_{\mathrm{imp}} = 0.1$ and $d/a = 0.1$.

We performed a number of tests to confirm the presence of this PCC. First of all, it exists up to $L = 3000a$ for various ribbon widths up to $N = 40$ for the potential range ($d/a = 1.5$). Moreover the PCC remains for LRI with $d/a = 2.0, 4.0, 6.0, 8.0$, and $u_0 = 1.0$, $n_{\mathrm{imp}} = 0.1$ and $N = 10$. As the effect is connected with the subtle feature of an excess mode in the band structure, it is natural that the result can only be valid for sufficiently weak potentials. For potential strengths comparable to the energy scale of the band structure, e.g. the energy difference between the transverse modes, the result should be qualitatively altered [81]. Deviations from the limit $\langle g \rangle \to 1$ also occur, if the incident energy lies at a value close to the change between $g = 2n - 1$ and $2n + 1$ for the ribbon without disorder. This is for example visible in the above calculations for $E = 0.4$ where the limiting value $\langle g \rangle < 1$ (figure 7(a)).

Turning to the case of SRI the inter-valley scattering becomes sizable enough to ensure TRS, such that the perfect transport supported by the effective chiral mode in a single valley ceases to exist. In figure 7(b), the nanoribbon length dependence of the averaged conductance for SRIs is shown. Since SRI causes inter-valley scattering for any incident energy, the electrons tend to be localized and the averaged conductance decays exponentially, $\langle g \rangle \sim \exp(-L/\xi)$, without developing a perfect conduction channel.

In this subsection, we have completely neglected the effect of electron–electron interaction, which may acquire the energy gap for non-doped zigzag nanoribbons at very low temperatures accompanying edge spin polarization [7, 21, 45]. In such a situation, a small transport gap will appear near $E = 0$. Since the edge states have less Fermi instability for the doped regime, the spin polarized states might be less important for the doped system.

3.4. Nearly pefect single-channel transport in disordered armchair nanoribbons

Now we turn to the discussion of the electronic transport properties of disordered metallic armchair nanoribbons. Figure 8(a) shows the averaged conductance $\langle g \rangle$ as a function of the ribbon length L in the presence of LRI for several different Fermi energies E. As we

can clearly see, the averaged conductance subjected to LRI in the single-channel transport ($E = 0.1, 0.2$ and 0.3) is nearly equal to one even in the long wire regime. This result is contrary to our expectation that electrons are scattered even by LRI, since wave functions at $\boldsymbol{K}_+$ and $\boldsymbol{K}_-$ points are mixed in armchair nanoribbons as we have already seen in section 2.2.2. For multi-channel transport ($E \geqslant 0.4$), the conductance shows a conventional decay. The robustness of single-channel transport can be clearly viewed from the Fermi energy dependence of conductance for several different ribbon lengths L as shown in figure 8(b). It should be noted that the energy dependence in the vicinity of $E = 0$ is quite different from that in zigzag nanoribbons. The conductance decays rapidly due to the finite ribbon width effect in zigzag ribbons [23], while the conductance around $E = 0$ remains unity in armchair ribbons (figure 8(b)).

Now let us see the effect of SRIs. Figure 8(c) shows the average conductance $\langle g \rangle$ as a function of the ribbon length L in the presence of SRI for several different Fermi energies E. In this case, the conductance decays exponentially even for single-channel transport. This result is similar to that previously obtained in zigzag nanoribbons. However, the rate of decay in the low-energy single-channel regime ($E = 0.1$ and 0.2) is slower than that for the multi-channel transport regime ($E \geqslant 0.4$) in this case. Similar results are obtained in [75], but in which only short-range disorder at the edge of ribbons is considered.

3.5. T-matrix analysis

The absence of localization in the single-channel region can be understood from the Dirac equation including the impurity potential term $\hat{U}_{\rm imp}$ with armchair edge boundary. To consider the amplitude of backward scattering, we introduce the T-matrix defined as

$$T = \hat{U}_{\rm imp} + \hat{U}_{\rm imp} \frac{1}{E - \hat{H}_0} \hat{U}_{\rm imp} + \cdots . \tag{35}$$

We can evaluate the matrix elements of $\hat{U}_{\rm imp}$ for the eigenstate $|n, k, s\rangle$ with the eigenenergy of equation (14) which can be written as

$$|n, k, s\rangle = \frac{1}{\sqrt{4WL}} \begin{pmatrix} \begin{pmatrix} s \\ \mathrm{e}^{-\mathrm{i}\theta(n,k)} \end{pmatrix} \mathrm{e}^{\mathrm{i}\kappa_n x} \\ \begin{pmatrix} -s \\ \mathrm{e}^{-\mathrm{i}\theta(n,k)} \end{pmatrix} \mathrm{e}^{-\mathrm{i}\kappa_n x} \end{pmatrix} \mathrm{e}^{\mathrm{i}ky}, \tag{36}$$

with the phase factor

$$\mathrm{e}^{-\mathrm{i}\theta(n,k)} = \frac{\kappa_n - \mathrm{i}k}{\sqrt{\kappa_n^2 + k^2}}. \tag{37}$$

Here it should be noted that the phase structure in equation (36) is different between $\boldsymbol{K}_+$ and $\boldsymbol{K}_-$ states, and these internal phase structures are critical for the scattering matrix elements of armchair nanoribbons, as we discuss in the following. Using the above expression, we can obtain the scattering matrix element

$$\langle n, k, s|\hat{U}_{\rm imp}|n', k', s'\rangle = \left(ss' + \mathrm{e}^{\mathrm{i}(\theta(n,k) - \theta(n',k'))}\right) V\left(n, k; n', k'\right), \tag{38}$$

with

$$V\left(n,k;n',k'\right)=\frac{1}{4WL}\int_0^W \mathrm{d}x\int_0^L \mathrm{d}y\,\mathrm{e}^{-\mathrm{i}(k-k')y}\left[u(\boldsymbol{r})\left(\mathrm{e}^{-\mathrm{i}(\kappa_n-\kappa_{n'})x}+\mathrm{c.c.}\right)\right.$$
$$\left.-\left(u'(\boldsymbol{r})\mathrm{e}^{-\mathrm{i}(\kappa_n+\kappa_{n'})x}+\mathrm{c.c.}\right)\right]. \tag{39}$$

It should be emphasized that equation (38) has the same form as that obtained for carbon nanotubes without inter-valley scattering ($u'_X(\boldsymbol{r})=0$) [5]. Interestingly, in spite of the fact that armchair nanoribbons inevitably suffer from inter-valley scattering due to the armchair edges ($u'_X(\boldsymbol{r})\neq 0$), we can express the matrix element for backward scattering as equation (38) by including $u'_X(\boldsymbol{r})$ into $V(n,k;n',k')$ in equation (39). This is due to the different phase structure between $\boldsymbol{K}_+$ and $\boldsymbol{K}_-$ in equation (36).

We focus on the single-channel regime where only the lowest subband with $n=0$ crosses the Fermi level. From equation (38), the scattering amplitude from the propagating state $|0,k,s\rangle$ to its backward state $|0,-k,s\rangle$ in the single-channel mode becomes identically zero, i.e.

$$\langle 0,-k,s|\hat{U}_{\mathrm{imp}}|0,k,s\rangle=0. \tag{40}$$

Thus, since the lowest backward scattering matrix element of T-matrix vanishes, the decay of $\langle g\rangle$ in the single-channel energy regime is extremely slow as a function of the ribbon length as we have seen in figure 8. However, the back-scattering amplitude in the second and much higher order does not vanish. Hence the single-channel conduction is not exactly perfect like carbon nanotubes [5], but *nearly* perfect in armchair nanoribbons.

4. Universality class

According to random matrix theory, ordinary disordered quantum wires are classified into the standard universality classes, orthogonal, unitary and symplectic. The universality classes describe transport properties, which are independent of the microscopic details of disordered wires. These classes can be specified by time-reversal and spin–rotation symmetry. The orthogonal class consists of systems having both time-reversal and spin–rotation symmetries, while the unitary class is characterized by the absence of TRS. The systems having TRS without spin–rotation symmetry belong to the symplectic class. These universality classes have been believed to inevitably cause Anderson localization although typical behaviors are different from class to class.

In the graphene system, the presence or absence of inter-valley scattering affects the TRS of the system. If inter-valley scattering is absent, i.e. $u'_X(\boldsymbol{r})=0$, the Hamiltonian $\hat{H}_0+\hat{U}_{\mathrm{imp}}$ becomes invariant under the transformation of $\mathcal{S}=-\mathrm{i}(\sigma^y\otimes\tau^0)C$, where C is the complex-conjugate operator. This operation corresponds to the special time-reversal operation for pseudospins within each valley, and supports that the system has symplectic symmetry. However, in the presence of inter-valley scattering due to SRI, the invariance under $\mathcal{S}$ is broken. In this case, the TRS across two valleys described by the operator $\mathcal{T}=(\sigma^z\otimes\tau^x)C$ becomes relevant, which indicates orthogonal universality class. Thus as noted in [72], graphene with LRI belongs to symplectic symmetry, but that with SRI belongs to orthogonal symmetry (see figure 9).

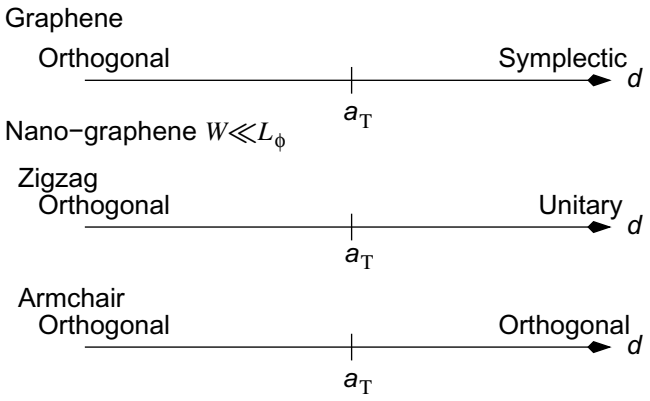

Figure 9. Summary concerning the universality crossover. On increasing the range of the impurity potential, graphene is known to be orthogonal for SRIs and symplectic for LRIs. However, zigzag nanoribbons are unitary class for SRIs. Armchair ribbons are classified into orthogonal class for the whole impurity range. L_ϕ is the phase coherence length. W is the width of graphene ribbons.

However, in the zigzag nanoribbons, the boundary conditions, which treat the two sublattices asymmetrically leading to edge states give rise to a single special mode in each valley. Considering now one of the two valleys separately, say the one around $k = k_+$, we see that the pseudo TRS is violated in the sense that we find one more left-moving than right-moving mode. Thus, as long as disorder promotes only intra-valley scattering, the system has no TRS. On the other hand, if disorder yields inter-valley scattering, the pseudo TRS disappears but the ordinary TRS is relevant making a complete set of pairs of time-reversed modes across the two valleys. Thus we expect to see qualitative differences in the properties if the range of the impurity potentials is changed.

The presence of one PCC has been recently found in disordered metallic carbon nanotubes with LRI [61]. The PCC in this system originates from the skew-symmetry of the reflection matrix, ${}^t\boldsymbol{r} = -\boldsymbol{r}$ [61], which is special to the symplectic symmetry with an odd number of channels. The electronic transport properties of such systems have been studied on the basis of the random matrix theory [62, 63]. On the other hand, zigzag ribbons without inter-valley scattering are not in the symplectic class, since they break TRS in a special way. The decisive feature for a PCC is the presence of one excess mode in each valley as discussed in the previous section.

In view of this classification we find that the universality class of the disordered zigzag nanoribbon with LRI potential (no inter-valley scattering) is the *unitary* class (no TRS). On the other hand, for SRI potentials with inter-valley scattering the disordered ribbon belongs to the *orthogonal* class (with overall TRS). Consequently, we can observe a crossover between two universality classes when we change the impurity range continuously.

However, in the disordered armchair nanoribbons, the special TRS within each valley is broken even in the case of LRI. This is because $u'_X(\boldsymbol{r}) \neq 0$ as we have seen in section 2.3. Thus, irrespective of the range of impurities, the armchair nanoribbons are classified into orthogonal universality class. *Since the disordered zigzag nanoribbons are classified into unitary class for LRI but orthogonal class for SRI* [23], *it should be noted that the universality crossover in a*

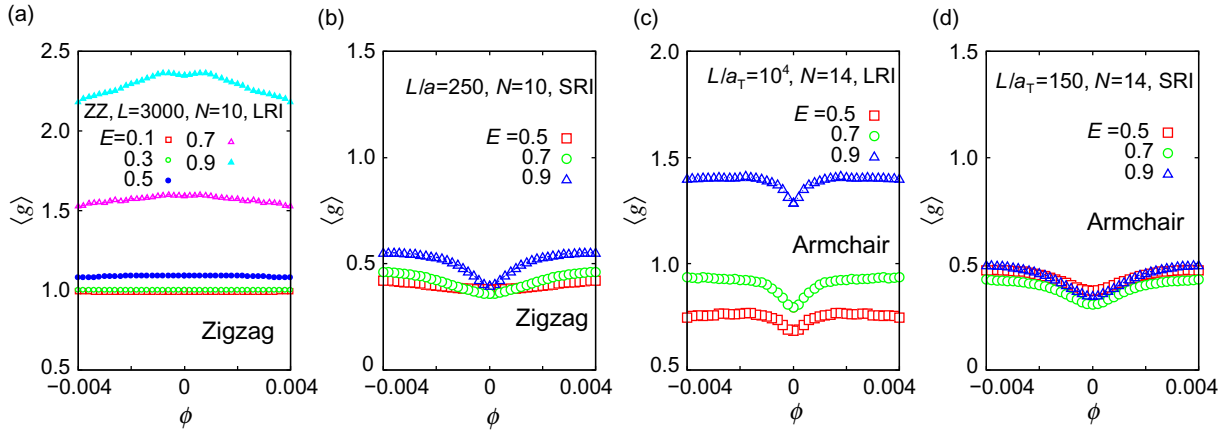

Figure 10. The magnetic field dependence of the averaged conductance for disordered zigzag nanoribbons with (a) LRIs and (b) SRIs. Similarly, the case for armchair nanoribbons with (c) LRIs and (d) SRIs. ϕ is the magnetic flux through a hexagonal ring, which is measured in units of ch/e.

nanographene system can occur not only due to the range of impurities but also due to the edge boundary conditions (see figure 9).

The application of a magnetic field enforces the above arguments. In figure 10, the magnetic field dependence of the averaged conductance for disordered zigzag nanoribbons with (a) LRIs and (b) SRIs is presented. Similarly, the case for armchair nanoribbons with (c) LRIs and (d) SRIs is presented. Here we have included the magnetic field perpendicular to the graphite plane, which is incorporated via the Peierls phase: $\gamma_{i,j} \rightarrow \gamma_{i,j} \exp\left[\mathrm{i}2\pi \frac{e}{ch} \int_i^j \mathrm{d}\boldsymbol{l} \cdot \boldsymbol{A}\right]$, where $\boldsymbol{A}$ is the vector potential. Since the time-reversal symmetry within the valleys for zigzag ribbons is already broken, the averaged conductance $\langle g \rangle$ for LRIs (absence of inter-valley scattering) is quite insensitive to the application of magnetic field as can be seen in figure 10(a). This is consistent with the behavior in the unitary class. For higher energies, weak magnetic field dependence appears due to inter-valley scattering. For all the other cases a weak magnetic field improves the conductance, i.e. weak localization behavior, which is typical for the orthogonal class.

5. Summary

In this paper, we have presented a brief overview of the electronic and transport properties of graphene nanoribbons focusing on the effect of edge shapes and impurity scattering. Concerning transport properties of disordered systems the most important consequence is the presence of a PCC in zigzag nanoribbons, i.e. the absence of Anderson localization that is believed to inevitably occur in the one-dimensional electron system. The origin of this effect lies in the single-valley transport, which is dominated by a chiral mode. On the other hand, large momentum transfer through impurities with short-range potentials involves both valleys, destroying this effect and leading to the usual Anderson localization. The obvious relation between chiral mode and TRS leads to the classification into unitary and orthogonal classes depending on the range of impurity potential. On the other hand, in spite of the lack of two well separated valley structures, the single-channel transport subjected to LRIs shows nearly

perfect transmission, where the backward scattering matrix elements in the lowest order vanish as a manifestation of internal phase structures of the wave function. These results are in contrast with the mechanism of PCC in disordered zigzag nanoribbons and metallic nanotubes where the well separation between two non-equivalent Dirac points is essential to suppress the inter-valley scattering.

Acknowledgments

This work was financially supported by a grand-in-aid for Scientific Research from the MEXT and the JSPS (nos 19710082, 19310094, 20001006 and 21540389).

References

[1] Novoselov K S *et al* 2004 *Science* **306** 666
Geim A K and Novoselov K S 2007 *Nat. Mat.* **6** 183
[2] Castro Neto A H, Guinea F, Peres N M, Novoselov K S and Geim A K 2009 *Rev. Mod. Phys.* **81** 109
[3] Novoselov K S *et al* 2005 *Nature* **438** 197
Zhang Y, Tan Y W, Stormer H L and Kim P 2005 *Nature* **438** 201
Novoselov K S *et al* 2006 *Nat. Phys.* **2** 177
[4] Ando T 2005 *J. Phys. Soc. Japan* **74** 777
[5] Ando T and Nakanishi T 1998 *J. Phys. Soc. Japan* **67** 1704
[6] Luk'yanchuk I A and Kopelevich Y 2004 *Phys. Rev. Lett.* **93** 166402
[7] Fujita M, Wakabayashi K, Nakada K and Kusakabe K 1996 *J. Phys. Soc. Japan* **65** 1920
[8] Nakada K, Fujita M, Dresselhaus G and Dresselhaus M S 1996 *Phys. Rev.* B **54** 17954
[9] Wakabayashi K, Fujita M, Ajiki H and Sigrist M 1999 *Phys. Rev.* B **59** 8271
[10] Wakabayashi K 2000 *PhD Thesis* University of Tsukuba http://www.tulips.tsukuba.ac.jp/dspace/handle/2241/2592
[11] Kobayashi Y *et al* 2005 *Phys. Rev.* B **71** 193406
Kobayashi Y *et al* 2006 *Phys. Rev.* B **73** 125415
[12] Niimi Y *et al* 2006 *Phys. Rev.* B **73** 085421
[13] Han M Y *et al* 2007 *Phys. Rev. Lett.* **98** 206805
[14] Li X *et al* 2008 *Science* **319** 1229
[15] Yang X *et al* 2008 *J. Am. Chem. Phys.* **130** 4216
[16] Jiao L *et al* 2009 *Nature* **458** 877
Kosynkin D V *et al* 2009 *Nature* **458** 872
[17] Jia X *et al* 2009 *Science* **323** 1701
[18] Wakabayashi K and Sigrist M 2000 *Phys. Rev. Lett.* **84** 3390
Wakabayashi K and Sigrist M 2001 *Phys. Rev.* B **64** 125428
[19] Wakabayashi K and Aoki T 2002 *Int. J. Mod. Phys.* B **16** 4897
[20] Rycerz A, Tworzydlo J and Beenakker C W J 2007 *Nature Phys.* **3** 172
[21] Son Y W, Cohen M L and Louie S G 2006 *Nature* **444** 347
[22] Kane C L and Mele E J 2005 *Phys. Rev. Lett.* **95** 226801
[23] Wakabayashi K, Takane Y and Sigrist M 2007 *Phys. Rev. Lett.* **99** 036601
Wakabayashi K, Takane Y and Sigrist M 2009 *Carbon* **47** 124
[24] Wakabayashi K 2003 *J. Phys. Soc. Japan* **72** 1010
[25] Beenakker C W J 2008 *Rev. Mod. Phys.* **80** 1337
[26] Akhmerov A R and Beenakker C W J 2007 *Phys. Rev.* B **75** 045426
Akhmerov A R and Beenakker C W J 2008 *Phys. Rev.* B **77** 205416
[27] Wakabayashi K and Sigrist M 2008 *J. Phys. Soc. Japan* **78** 034717

[28] Katsnelson M I, Novoselov K S and Geim A K 2006 *Nat. Phys.* **2** 620
[29] Nakabayashi J 2009 *Phys. Rev. Lett.* **102** 066803
[30] Cresti A *et al* 2008 *Phys. Rev.* B **77** 233402
Cresti A *et al* 2008 *Nanotechnology* **19** 265401
Cresti A *et al* 2009 *Phys. Rev.* B **79** 233404
[31] Zârbo L P and Nikolić B K 2007 *Europhys. Lett.* **80** 47001
Dragomirova R L *et al* 2009 *Phys. Rev.* B **79** 241401
[32] Abanin D A and Levitov L S 2007 *Science* **317** 641
[33] Morooka M *et al* 2008 *Phys. Rev.* B **77** 033412
Souma S *et al* 2006 *J. Surf. Sci. Nanotechnol.* **4** 78
[34] Peres N M R 2009 *J. Phys: Condens. Matter* **21** 323201
[35] Ryzhii V *et al* 2008 *J. Appl. Phys.* **104** 114505
Ryzhii V *et al* 2008 *J. Appl. Phys.* **103** 094510
[36] Wimmer M *et al* 2008 *Phys. Rev. Lett.* **100** 177207
[37] Williams J R 2007 *Science* **317** 638
[38] Molitor F *et al* 2007 *Phys. Rev.* B **76** 245426
[39] Wang X *et al* 2008 *Phys. Rev. Lett.* **100** 206803
[40] Tapaszto L *et al* 2008 *Nat. Nanotechnol.* **3** 397
[41] Stampfer C *et al* 2009 *Phys. Rev. Lett.* **102** 056403
[42] Chen Z *et al* 2007 *Physica* E **40** 228
[43] Campos L *et al* 2009 *Nano Lett.* **9** 2600
[44] Miyazaki H *et al* 2008 *Appl. Phys. Exp.* **1** 024001
[45] Wakabayashi K, Sigrist M and Fujita M 1998 *J. Phys. Soc. Japan* **67** 2089
[46] Kusakabe K and Maruyama M 2003 *Phys. Rev.* B **67** 092406
[47] Wakabayashi K *et al* 2003 *J. Phys. Soc. Japan* **72** 998
[48] Yamashiro A *et al* 2003 *Phys. Rev.* B **68** 193410
[49] Harigaya K and Enoki T 2002 *Chem. Phys. Lett.* **351** 128
[50] Yoshioka H 2003 *J. Phys. Soc. Japan* **72** 2145
[51] Hikihara T *et al* 2003 *Phys. Rev.* B **68** 035432
[52] Palacios J J, Fernández-Rossier J and Brey L 2008 *Phys. Rev.* B **77** 195428
[53] Fernández-Rossier J and Palacios J J 2007 *Phys. Rev. Lett.* **99** 177204
[54] Sasaki K I and Saito R 2008 *J. Phys. Soc. Japan* **77** 054703
[55] Kumazaki H and Hirashima D S 2008 *J. Phys. Soc. Japan* **77** 044705
[56] Hod O *et al* 2008 *Phys. Rev.* B **77** 035411
Hod O *et al* 2007 *Nano Lett.* **7** 2295
Hod O *et al* 2007 *Phys. Rev.* B **76** 233401
[57] Ezawa M 2008 *Physica* E **40** 1421
Ezawa M 2007 *Phys. Rev.* B **76** 245415
[58] Kundin K N 2008 *ACS Nano* **2** 516
[59] Wassmann T *et al* 2007 *Phys. Rev. Lett.* **101** 096402
[60] Shemella P 2007 *Appl. Phys. Lett.* **91** 042101
[61] Ando T and Suzuura H 2002 *J. Phys. Soc. Japan* **71** 2753
[62] Takane Y 2004 *J. Phys. Soc. Japan* **73** 9
[63] Sakai H and Takane Y 2005 *J. Phys. Soc. Japan* **75** 054711
[64] Hirose K, Ohtsuki T and Slevin K 2008 *Physica* E **40** 1677
[65] Takane Y and Wakabayashi K 2007 *J. Phys. Soc. Japan* **76** 053701
[66] Beenakker C W J 1997 *Rev. Mod. Phys.* **69** 731–808
[67] Yamamoto M, Takane Y and Wakabayashi K 2009 *Phys. Rev.* **79** 125421
[68] Wallace P R 1947 *Phys. Rev.* **71** 622

[69] Fujita M, Igami M and Nakada K 1997 *J. Phys. Soc. Japan* **66** 1864
[70] Son Y M, Cohen M L and Louie S G 2006 *Phys. Rev. Lett.* **97** 216803
[71] Brey L and Fertig H A 2006 *Phys. Rev.* B **73** 235411
[72] Suzuura H and Ando T 2002 *Phys. Rev. Lett.* **89** 266603
[73] Büttiker M, Imry Y, Landauer R and Pinhas S 1985 *Phys. Rev.* B **31** 6207
[74] Ando T 1991 *Phys. Rev.* B **44** 8017
[75] Li T C and Lu S P 2008 *Phys. Rev.* B **77** 085408
[76] Louis E, Vergés J A, Guinea F and Chiappe G 2007 *Phys. Rev.* B **75** 085440
[77] Mucciolo E R, Castro Neto A H and Lewenkopf C H 2009 *Phys. Rev.* B **79** 075407
[78] Miyamoto Y, Nakada K and Fujita M 1999 *Phys. Rev.* B **59** 9858
[79] MacDonald A H 1984 *Phys. Rev.* B **29** 6563–9
[80] Ishizaka S, Nakamura K and Ando T 1993 *Phys. Rev.* B **48** 12053–62
[81] Wakabayashi K 2002 *J. Phys. Soc. Japan* **71** 2500